Aharonov-Bohm-type oscillations in antidot lattices in the quantum Hall regime

Masanori Kato,[*] Akira Endo, Shingo Katsumoto, and Yasuhiro Iye

Institute for Solid State Physics, University of Tokyo, Kasshiwa, Chiba 277-8581, Japan

Various aspects of the Aharonov–Bohm(AB)-type effects in antidot lattices in the quantum Hall (QH) regime are studied. Features associated with spin-resolved edge channels formed around the antidots are observed in the vicinity of the $\nu=2$ [ν being the Landau level (LL) filling factor] QH state. AB-type oscillations with anomalous periodicities lying between $h/2e$ and $h/3e$ are observed on the higher field side of the $\nu=2$ QH state. The phenomenon is interpreted basically as $h/2e$ oscillation reported earlier for single antidot systems, but with important modification specific to the antidot array system. By tuning the negative front gate bias, different regimes of relative importance of the intra- and inter-LL tunnelings are explored.

I. INTRODUCTION

Artificially fabricated structures based on GaAs/AlGaAs two-dimensional electron system (2DES) have been used to explore various aspects of electron transport in tailored potential landscapes. One of such artificial structures is an antidot lattice, i.e., a regular array of potential hills inaccessible to 2D electrons. Electrons travel through regions between antidots and (if the 2DES is sufficiently clean and impurity scattering is infrequent) are scattered by the antidot and sample boundaries, which result in ballistic transport.[1] A key parameter characterizing an antidot lattice is the aspect ratio, or the ratio between the antidot diameter and the lattice period. An antidot lattice with a small aspect ratio can be viewed as a 2DES subjected to a periodic array of scatterers, i.e., a ballistic pinball situation.[2] On the other hand, one with a large aspect ratio is more like a network of narrow channels formed between the antidots.[3] A magnetic field perpendicular to the 2DES plane introduces another length scale, i.e., the cyclotron radius, to the system. Various magnetotransport phenomena depending on the relation between these length scales have been uncovered. In the low field regime, where the cyclotron radius is larger or comparable to the antidot lattice period, geometrical resonance effect manifests itself as $1/B$-periodic commensurability oscillations of magnetoresistance.[1–3] It has been elucidated that the chaotic or nonchaotic nature of the electron trajectories plays a crucial role in the phenomenon.[4,5] At higher magnetic fields, where the cyclotron radius becomes smaller than the interantidot spacing, Shubnikov–de Haas oscillations take over. In the quantum Hall (QH) regime, edge states are formed along the edge of the sample and around the antidots. Transport in this regime is governed by the presence (or absence) of extended states at the Fermi level.

In systems with a large aspect ratio, the magnetoresistance exhibits the so-called Aharonov–Bohm (AB)-type oscillations both in the low magnetic field region[4,6–8] and in the quantum Hall regime.[8–12] They will be hereafter called low field AB-type oscillation (LFABO) and high field AB-type oscillation (HFABO), respectively. These osillations are B periodic with the period corresponding to one flux quantum per *relevant* area. The relevant area is the unit cell of the antidot lattice for LFABO, while it is the area of an antidot

(with an appropriate correction for the width of the peripheral depletion region) for HFABO. The AB-type effect in a large array of antidots differs from that in a single ring,[13] because the AB interference effect in the latter should be smeared by statistical averaging in a large ensemble.[14] Theoretical analyses of the situations corresponding to LFABO using numerical simulations have shown that the AB-type oscillations reflect fine structures in the electronic density of states originating from the quantization of electron orbits pinned around antidots.[4,5,15] The origin of HFABO is less elucidated, although there are a few theoretical studies on antidot arrays in high magnetic fields.[15–17] The purpose of the present study is to elucidate various aspects of the AB-type oscillation effect in antidot lattices in the QH regime.

In high magnetic fields, the energy spectrum of 2DES is quantized into a series of spin-split Landau levels (LLs). In the $\nu=2$ QH regime, for instance, two spin-resolved edge states of the lowest LL are formed around the antidots. A peculiar frequency-doubling phenomenon has been observed in this regime, which is attributed to the spin-resolved edge states.[9] Related phenomena are also reported in single antidot samples.[18–22] In the present experiment, we have found that the HFABO in the vicinity of the $\nu=2$ QH resistance minimum exhibits an anomalous periodicity. We have investigated the evolution of the anomalous HFABO as well as the regular HFABO with the front gate bias, to gain some insights into their origins. We discuss the relation between the newly found anomalous HFABO and those previously reported.

II. EXPERIMENTAL METHOD

Antidot lattice samples were fabricated from GaAs/AlGaAs single heterojunction wafers (density $n=4.0\times10^{15}$ m^{-2} and mobility $\mu=98$ m^2/V s). The heterointerface (the 2DES plane) was located at 60 nm from the surface. Using electron beam lithography and shallow ($\sim$30 nm) wet chemical etching, square arrays of antidots, as shown in Fig. 1(a), were fabricated on the active area of a Hall bar sample with AuGe/Ni Ohmic contact pads. The antidot pattern and the Hall bar shape were fabricated in a single lithography process so as to ensure good registry of
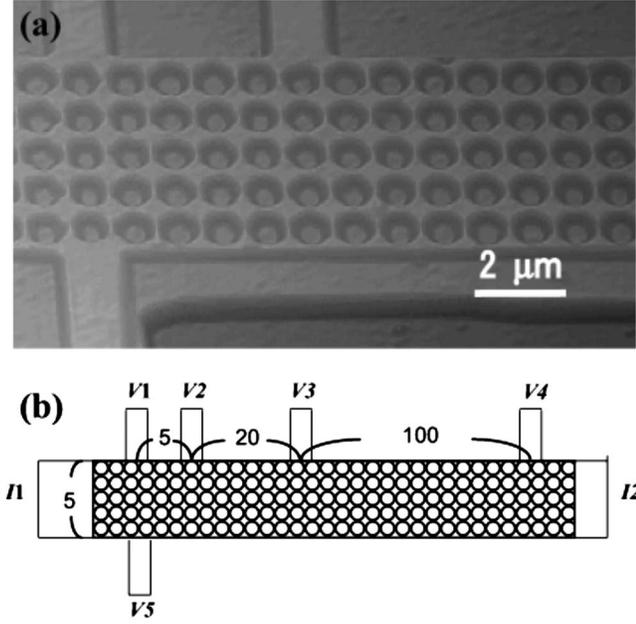
FIG. 1. (a) An atomic force microscopy image of the Hall bar sample with antidot lattice. (b) The probe assignment of the sample (the width of the Hall bar is 5.3 μm). The figure in the Hall bar indicates the number of antidots.

the structure. Antidots of radius $r=350$ nm were regularly placed with lattice period $a=1$ μm. The effective radius r^* of antidots is the lithographical radius r plus the width of depletion region, which is on the order of 100 nm. The effective aspect ratio is, therefore, ~ 0.9, which puts the present antidot samples in the large-aspect-ratio category. A Au-Ti Schottky front gate enabled us to change the Fermi level of the system. The sample shape was an elongated Hall bar with five antidots across the width, as shown in Fig. 1(b). The voltage probes were placed along the length of the Hall bar so as to monitor three segments consisting of different numbers of antidot columns (5, 20, and 100). The voltages across the different probes were simultaneously measured in order to check the reproducibility of the phenomena. The results presented in this paper are not specific to any particular array, but are commonly observed in all segments except for minor differences, for example, in the amplitude of oscillation. Samples were mounted on a rotating stage of a top-loading probe and directly inserted to the mixing chamber of a dilution refrigerator with a base temperature 30 mK. Magnetic fields up to 15 T were applied perpendicular to the 2D plane. Magnetoresistivity ρ_{xx} and Hall resistivity ρ_{xy} were measured by a standard low frequency (13 Hz) ac lock-in technique with a typical excitation current of 1 nA. In what follows, ρ_{ij} denotes the four terminal resistivity obtained by passing current between the contacts I_1 and I_2 and measuring the voltage between the contacts V_i and V_j.

III. RESULTS AND DISCUSSION

A. Overview of the high field Aharonov–Bohm-type oscillations effects in various field ranges

Prior to getting into detailed discussions, it is helpful to have an overview of the AB-type effects over the entire mag-
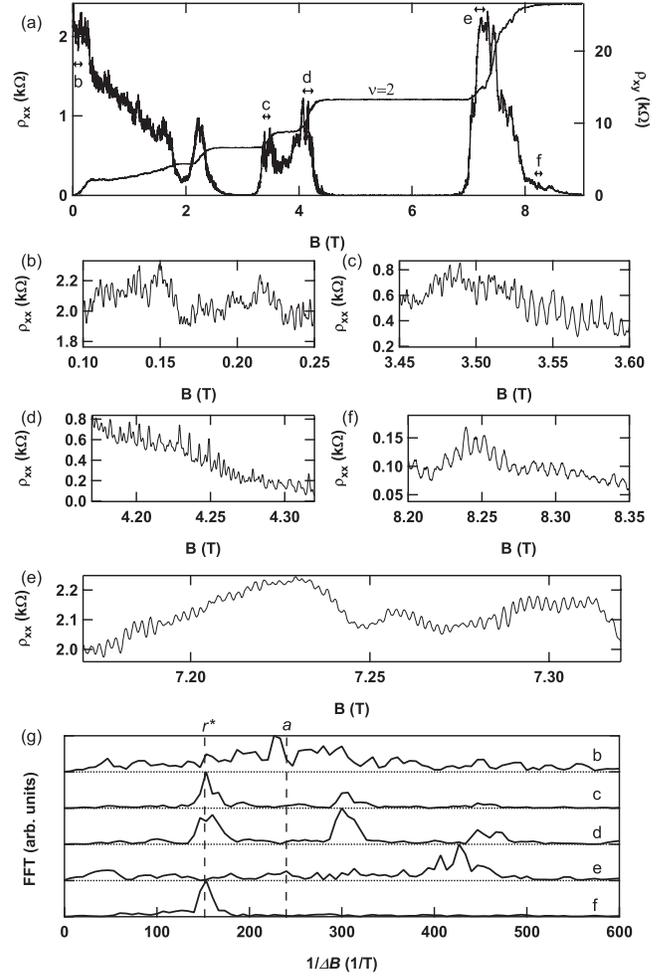

FIG. 2. (a) Traces of ρ_{xx} and ρ_{xy} for a 5×5 array under zero front gate bias ($V_g=0$ V). [(b)–(f)] Expanded ρ_{xx} traces for the field ranges labeled b–f in (a). Note that the magnetic field scale of (e) is different from the other figures. (g) The Fourier power spectra corresponding to the data of (b)–(f). The vertical dashed lines indicate the calculated positions of the peak corresponding to the antidot area πr^{*2} for the effective radius $r^*=450$ nm and the unit cell area a^2 ($a=1$ μm).

netic field range investigated. Figure 2(a) shows the magnetoresistivity $\rho_{xx}(=\rho_{12})$ and the Hall resistivity $\rho_{xy}(=\rho_{15})$ obtained from the 5×5 antidot array under zero front gate bias ($V_g=0$ V). The ρ_{xx} trace exhibits oscillatory behavior at various magnetic fields ranging from zero to the $\nu=1$ QH regime. Figures 2(b)–2(f) are the expanded traces of ρ_{xx} in the specific magnetic field ranges indicated in Fig. 2(a) by b–f, respectively. The Fourier power spectra for the respective field ranges are given in Fig. 2(g).

Figure 2(b) shows the LFABO in the field range $B\simeq0.2$ T, where the so-called commensurability peak of magnetoresistance, associated with the matching of cyclotron diameter with the superlattice period a, occurs. (The cyclotron radius at $B=0.2$ T is $R_c=435$ nm.) The ρ_{xx} exhibits oscillatory behavior, whose Fourier power spectrum has a broad peak centered around 250 T^{-1}. The resistance fluctuations in this regime contain both the LFABO and the so-called universal conductance fluctuations. In the case of
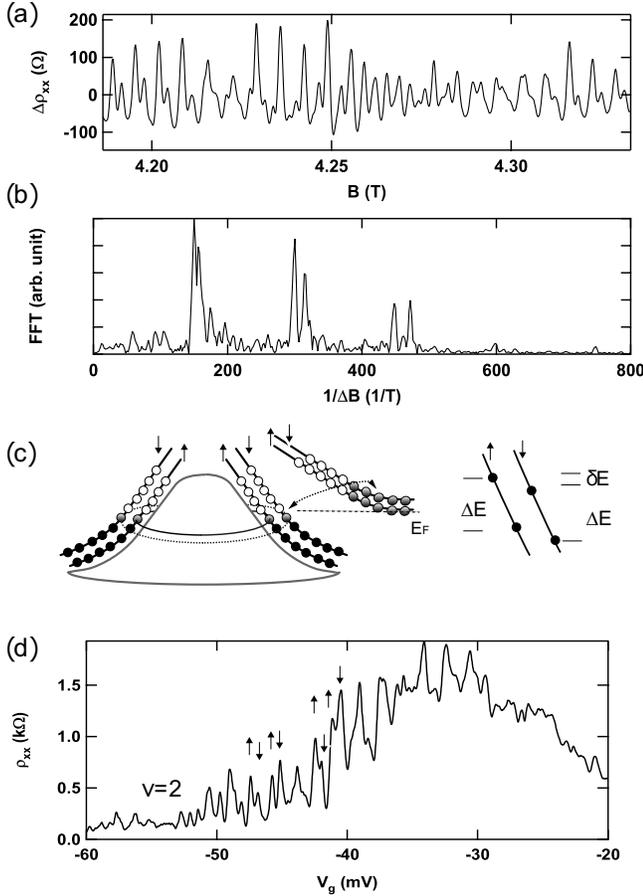
FIG. 3. (a) The oscillatory component of the trace in Fig. 2(d) after subtraction of the smooth background. (b) Fourier power spectrum obtained from (a) in the field range $4.0 < B < 4.5$ T. The two peaks at 150 and 157 T^{-1} and their higher harmonics are seen. (c) Left: schematic drawing of the single particle states encircling the antidot in the QH transition regime between $\nu=2$ and 3. The solid, open, and half-filled dots represent occupied, unoccupied, and partially occupied states, respectively. There are also extended states in the bulk region. Right: relation between spin-resolved single particle energy levels near the Fermi energy. ΔE is the energy separation of each SP state with the same spin and δE is the energy separation between the spin-up and spin-down SP states. (d) Gate voltage dependence of the ρ_{12} at $B=3.4$ T, which show paired peaks marked with up and down arrows around -40 mV.

larger arrays of antidots,[8,12] the LFABO is more conspicuous. The AB-type oscillation period $\Delta B \simeq 4$ mT in this field range is consistent with the condition that the magnetic flux enclosed within the unit cell of the square antidot lattice changes by a single flux quantum, i.e., $\Delta B = (h/e)/a^2$ with $a=1$ μm. As elucidated by theoretical studies using numerical simulations,[4,5] the LFABO is manifestation of the oscillatory fine structures of the density of states. In the field range $0.3 \lesssim B \lesssim 2$ T, where ρ_{xx} exhibits the Shubnikov–de Haas oscillations, the period of the AB-type oscillations gradually increases with B. This reflects a gradual transition of the AB period from $\Delta B = (h/e)/a^2$ (associated with the unit cell area) to $\Delta B = (h/e)/(\pi r^{*2})$ (associated with the effective antidot area), and corresponds to crossover from the

LFABO to the HFABO, as detailed in our previous papers.[8,12]

In the QH regime, edge channels are formed both along the sample edges and around individual antidots. (The magnetic length $\ell_B = \sqrt{\hbar/eB}$ at $B=4$ T is $\ell_B=13$ nm, so that the description in terms of edge states around each antidot should be an appropriate picture.) Single particle (SP) states localized around each antidot are quantized so as to enclose integer magnetic flux quanta, $B\pi r^{*2}=m(h/e)$ (m: integer), according to the Bohr–Sommerfeld quantization condition. When B is adiabatically increased (decreased), the number of the enclosed flux quanta is conserved, so that the radius r^* of the SP state decreases (increases) and the individual SP states move up (down) in energy. Alternatively, the electrochemical potential can be swept by changing the gate bias at a fixed B. It is the one-by-one crossing of these SP states through the Fermi level that gives rise to the HFABO manifested in the macroscopic transport.[10] The ρ_{xx} trace in the QH plateau transition region contains clear B-periodic oscillations. The canonical cases are shown in Figs. 2(c) and 2(f), which we shall call *normal* HFABO hereafter. The corresponding Fourier spectra given in Fig. 2(g) are simple with the fundamental HFABO frequency ~ 150 T^{-1} (period $\Delta B=6.5$ mT). The effective antidot radius r^* calculated from the relation $\Delta B = (h/e)/(\pi r^{*2})$ is $r^*=450$ nm. This value is in reasonable agreement with the lithographical radius $r=350$ nm of the antidot plus the width (~ 100 nm) of the depletion region. The Fourier spectrum for (c) contains higher harmonic components, which reflect reflecting multiple circumnavigation of electrons around the antidots.

In contrast to the normal behavior of HFABO in Figs. 2(c) (LL filling $\nu \sim 3.5$) and 2(f) ($\nu \sim 1.5$), the HFABO on both sides of the $\nu=2$ QH state [Figs. 2(d) and 2(e)] exhibits exotic features. Figure 2(d) shows the ρ_{xx} trace on the lower field side of $\nu=2$. The Fourier spectrum of HFABO in this range exhibits a characteristic double-peak structure. On the higher field side of $\nu=2$ [Fig. 2(e)], the periodicity of the HFABO is anomalous, as evident from the corresponding Fourier spectrum. In what follows, we discuss the origins of these exotic features in the vicinity of the $\nu=2$ QH state.

B. Spin-split high field Aharonov–Bohm-type oscillations on the lower field side of $\nu=2$ at zero gate bias

Figure 3(a) shows the oscillatory component of Fig. 2(d), which exhibits a series of twin peaks. The twin-peak structure changes with magnetic field in such a way that the HFABO trace over a wider range displays a beating pattern. This is reflected in the Fourier spectrum [Fig. 3(b)], which shows a paired peak with AB frequencies of 150 and 157 T^{-1}. The corresponding effective radii are $r^*=440$ and 450 nm. The two values of r^* indicate involvement of two edge channels around the antidot, which can be naturally attributed to the spin-resolved pair of the $N=0$ edge channel, as schematically depicted in Fig. 3(c). The SP states for the up-spin and down-spin electrons are at different energies, as shown in the figure, where ΔE is the energy separation between two successive SP states, and $\delta E = g\mu_B B$ is the Zeeman splitting of each orbital state.

Figure 3(d) shows the variation of ρ_{12} when the front gate bias is swept under a fixed magnetic field $B=3.4$ T to traverse the QH plateau transition between $\nu=2$ and $\nu=3$. The oscillatory structure arises from successive passing of individual SP states through the Fermi level. The oscillation period reflects the energy spacing of the adjacent SP states ΔE (multiplied by a conversion factor from the front gate bias change to the electrochemical potential shift of the 2DES). The observed value $\Delta V_g \simeq 2.0$ mV is similar to those found in our previous studies.[8,10] There are a series of paired peaks (indicated by the up and/or down arrows) in the range $-50 < V_g < -40$ mV, which fit well with the above picture of spin-resolved edge states.

In the QH plateau transition regime between $\nu=2$ and 3, the edge states of the $N=0$ LL encircle the antidots and the extended states of the $N=1$ LL spread through the bulk, as depicted in Fig. 3(c). The latter are responsible for the finite conductivity and their coupling with the former gives rise to the HFABO. The reason why the spin-resolved HFABO can be observed in this region lies in the fact that the spin splitting of these LLs is neither too small nor too large. With the spin splitting not too large, the extended states contain both spin-up and spin-down electrons of the $N=1$ LL, as inferred from the finite conductivity in the $\nu=3$ QH region [see Fig. 2(a)]. Thus, the coupling occurs both between the $(0, \uparrow)$ edge state and the $(1, \uparrow)$ bulk state, and between the $(0, \downarrow)$ edge state and the $(1, \downarrow)$ bulk state. The comparable amplitude of the two oscillations [as seen in the Fourier spectrum of Fig. 3(b)] suggests that the typical tunneling distances are comparable for the both processes. This picture is in accordance with the observations that the two oscillation components smear out equally with temperature (not shown), and that the HFABO is visible up to the center of the QH plateau transitions. The paired-peak structure disappears in the filling range between $\nu=3$ and 4 [Fig. 2(c)], where only the $(1, \downarrow)$ LL exists as the bulk extended state.

C. $h/2e$ oscillations on the higher field side of $\nu=2$ under strong depletion

The spin-split HFABO discussed above occurs in the QH plateau transition region between $\nu=2$ and 3, and originates from the coupling between the edge states and the bulk extended states. Nearer to the center of the $\nu=2$ QH state, the $N=1$ LLs move far above the Fermi level, so that ρ_{xx} vanishes and the HFABO becomes invisible. When a large negative voltage is applied to the front gate, all the QH features are shifted to lower magnetic fields and, concomitantly, ρ_{xx} becomes nonzero even near the center of the QH state. In such a situation, a different type of spin-split HFABO is observed.

Figure 4(a) shows a part of the ρ_{13} trace in the higher field side of the $\nu=2$ QH state under a large negative gate bias $V_g=-70$ mV. The HFABO on the lower field side of this trace (denoted with α and β) is rich in the second harmonic component, while that on the higher field side (denoted with γ) contains only the fundamental frequency. The three panels of Fig. 4(b) show the Fourier spectra taken from the ρ_{xx} trace in the three intervals indicated in Fig. 4(a). Figure 4(c) shows
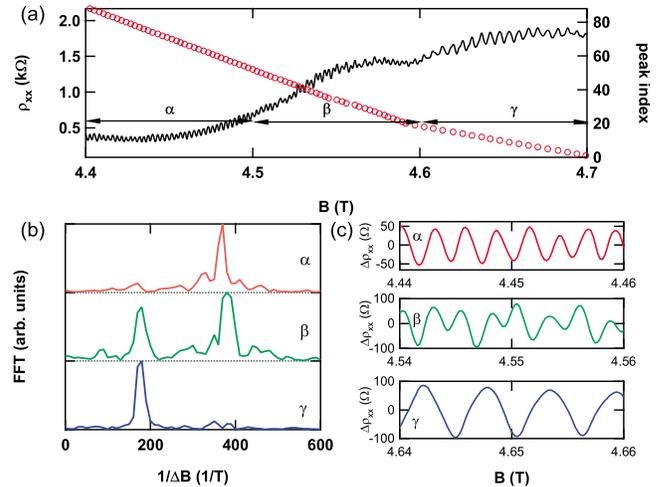

FIG. 4. (Color online) (a) ρ_{13} trace at $V_g=-70$ mV between $\nu=1$ and 2 ($\nu=2$ at $B\approx4$ T) with the index plot of the peak positions (red circles). (b) Fourier power spectra and the oscillatory component taken from the oscillations in the three magnetic field ranges marked with α, β, and γ in (a). (c) Representative segments of the ρ_{13} trace in each of the three field ranges.

representative segments of the ρ_{xx} trace in the respective ranges. The HFABO in the range $4.4 < B < 4.5$ T is almost pure $h/2e$ oscillation, as seen in the top panels of Figs. 4(b) and 4(c).

Similar double-frequency AB oscillations are reported for single antidot systems.[18–20,22] Ford *et al.*[18] observed $h/2e$ AB oscillations in a tunable single antidot sample around $\nu=2$, where two (spin-up and -down) edge states are formed around the antidot. Kataoka *et al.*[20] explained the phenomenon by considering the Coulomb blockade effect on the electron tunneling between the compressible rings formed around the antidot. The model asserts that self-consistent screening upon electron tunneling into (out of) the outer spin edge state combined with spin-flip process between the inner and outer edge states leads to two resonance per h/e period. To avoid terminological confusion, the *outer* edge state means the one further from the geometrical edge of the antidot. It is this outer edge state that governs the AB periodicity. This point is practically insignificant for the single antidot system, because the area enclosed by the outer edge is not much different from that by the inner edge state. However, it is crucial in the context of exotic HFABO periodicity in the antidot array to be discussed in the next subsection.

It is natural to consider the $h/2e$ HFABO presently observed in the antidot array samples to be the same origin in its basic essence. Whether exactly the same argument applies to the present case of antidot array should be scrutinized. The effectiveness of Coulomb charging effect depends on the confinement size. As regards the antidot size, the present antidots are larger than the above-mentioned single antidots (by a factor of 2–3 in linear dimension).[18–20] On the other hand, the 2DES carrier density is larger up to a factor of 2 for the present case than the single antidots. This leads to a higher magnetic field range for the same LL filling, and accordingly a smaller magnetic length. The Coulomb energy is also affected by the presence of the metallic gate.

Although precise evaluation is difficult, the differences in the relevant parametes fall within a factor of 3 and some of them counteract with others, so that the overall magnitude of the charging effect should be comparable.

An important difference between the charging effect in a single antidot and that in an antidot array lies in the interantidot tunneling for the latter case. Whether interantidot tunneling occurs as an incoherent process or there is any synchronization mechanism is an interesting issue to be explored. In regard to this point, a question may be raised if the presently observed phenomena may originate not from the sample in total but from a small part of the sample (possibly just a single antidot). However, this is highly unlikely because the essential features described above were consistently observed regardless of the combination of the voltage probes. We believe that the observed $h/2e$ HFABO is an intrinsic property of the antidot array.

When the system moves further toward $\nu=1$, there is a clear crossover of the HFABO from the $h/2e$ period to the h/e period at around $B=4.6$ T. The HFABO above this field is a simple h/e oscillation, as seen in the bottom panels of Figs. 4(b) and 4(c). We shall return to the HFABO phenomena in this filling factor range in the next subsection.

D. High field Aharonov–Bohm-type oscillations with anomalous period on the higher field side of $\nu=2$ at zero gate bias

Let us now turn to the anomalous behavior of HFABO on the higher field side of $\nu=2$ under zero gate bias ($V_g=0$ V). As already shown in Fig. 2(e), the HFABO in this range exhibits an exotic periodicity. The Fourier spectrum has a peak around $(\Delta B)^{-1} \sim 420$ T^{-1}, which is an anomalous value lying halfway between $h/2e$ and $h/3e$ and bearing no simple relationship with the antidot area or its multiples. As is evident in Fig. 2(e), this exotic HFABO manifests itself as a regular oscillation over a considerable range of magnetic field. It should be remarked that this exotic HFABO phenomenon is not a single anomaly observed in a specific sample. Similar exotic AB periods between $h/2e$ and $h/3e$ have been observed in the same filling factor range in other samples with antidot radii $r=350$ and 300 nm.[11,12]

In order to gain insight into this phenomenon, we investigated how this exotic periodicity changes with magnetic field and gate bias. Figure 5(a) shows the same ρ_{xx} trace as Fig. 2, in the field range in which the exotic HFABO is observed [region "e" in Fig. 2(a)]. The circles indicate the AB period ΔB_{ex} extracted from the field range indicated by the horizontal bar. It is seen that the *exotic* AB period ΔB_{ex} decreases with increasing magnetic field.

Figure 5(b) shows the gate bias dependence of the normal and exotic AB periods. The open symbols represent the evolution of the normal AB period taken from the normal HFABO on the lower field side of $\nu=2$ (more specifically $\nu \sim 2.6$). The normal AB period ΔB_{nm} becomes smaller for a more negative gate bias, as expected, because a more negative bias implies a wider depletion area and hence a larger effective antidot radius. The behavior of the exotic HFABO is opposite. Solid symbols represent the evolution of the exotic AB period ΔB_{ex} with the front gate bias V_g. This evolu-
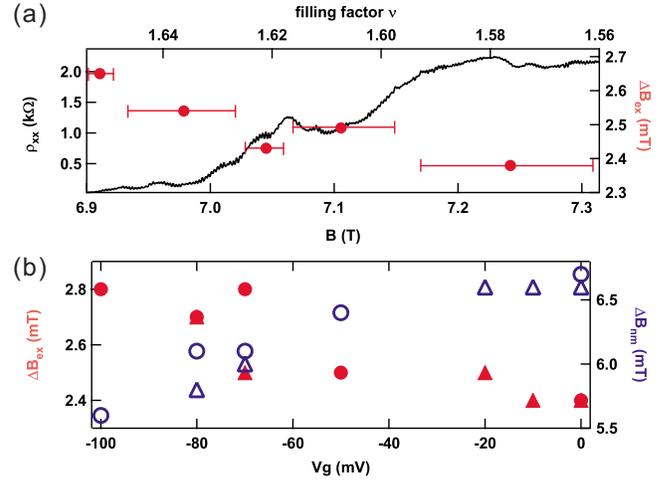

FIG. 5. (Color online) (a) ρ_{12} trace on the higher field side of $\nu=2$ at $V_g=0$ V. The circles represent the period of AB-type oscillations in each magnetic field range. (b) The AB periods in different ranges of the front gate bias. (Note that the magnetic field range, in which the HFABO is visible, also changes with the gate bias.) Open symbols represent ΔB_{nm}, the period of the normal HFABO, on the lower field side of $\nu=2$. Solid symbols represent ΔB_{ex}, the period of the exotic HFABO on the higher field sid of $\nu=2$. Circles and triangles represent the data taken in separate runs after different cooldowns.

tion of ΔB_{ex} with V_g actually arises from the shift in the field range, in which the HFABO is visible, i.e., the data point at $V_g=0$ V is obtained from the filling range near $\nu \sim 1.6$, while that at $V_g=-100$ mV from $\nu \sim 1.8$. Together with the magnetic field dependence shown in Fig. 5(a), the trend is that ΔB_{ex} decreases with decreasing ν. An important point to note is that the ΔB_{ex} evolves continuously from 2.38 mT ($\sim h/2.35e$) at $V_g=0$ V to 2.8 mT (close to $h/2e$) at $V_g=-100$ mV.

Figure 6 schematically illustrates the edge states formed around the antidots in the relevant filling factor range. The two figures represent the cases of weak and strong depletions. In this filling factor range (ν somewhat smaller than 2), the $(0, \uparrow)$ LL is bound to the antidot, while the $(0, \downarrow)$ LL is either bound or on the verge of delocalization. The range of ν, in which ρ_{xx} becomes nonzero and the HFABO becomes visible, depends on the degree of depletion, i.e., the narrow-
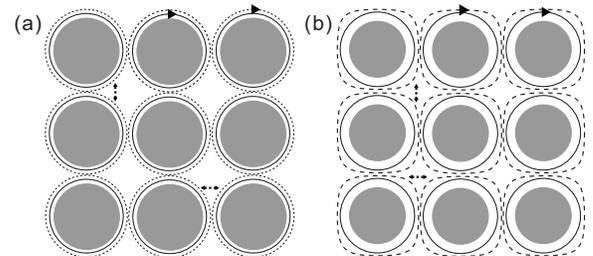

FIG. 6. Schematic illustrations of the localized channels around antidots on the higher field side of the $\nu=2$ plateau for (a) strongly depleted case (large negative V_g) and (b) weakly depleted case ($V_g \sim 0$). Solid curves represent the $(0, \uparrow)$ edge channels and dashed curves represent the $(0, \downarrow)$ edge channels.

ing of the constriction between the antidots. The filling factor range, where the exotic HFABO becomes conspicuous, changes from $\nu \sim 1.8$ at $V_g = -100$ mV to $\nu \sim 1.6$ at $V_g = 0$ V. In the strong depletion regime [Fig. 6(a)], the constriction between the antidots is narrow enough to allow intra-LL tunneling between the localized $(0, \downarrow)$ edge states already at around $\nu = 1.8$. In this case, the area enclosed by the $(0, \downarrow)$ edge states is close to the antidot area. Indeed, the period of the exotic HFABO at $V_g = -100$ mV is close to $h/2e$, as seen in Fig. 5(b). As the V_g is made less negative, the filling factor ν at which the exotic HFABO occurs shifts progressively to lower values. The $(0, \downarrow)$ edge states tend to be more delocalized in the relevant filling factor range, so that the relevant area becomes larger as schematically illustrated in Fig. 6(b). The decreasing trend of the exotic AB period from $h/2e$ at $V_g = -100$ mV to lower values at less negative V_g is interpreted in this picture. The deformed circles drawn with a dashed line in Fig. 6(b) show the image of the $(0, \downarrow)$ edge states corresponding to the effective area of 0.87 μm^2 calculated from $\Delta B = 2.38$ mT for the case of $V_g = 0$ V.

E. High field Aharonov–Bohm-type oscillations on the lower field side of $\nu = 1$

Finally, we discuss the HFABO in the QH plateau transition region between $\nu = 1$ and 2. As already seen in Fig. 2(f), the HFABO in this regime occurs with the basic h/e periodicity. The amplitude of the HFABO in this region (lower field side of $\nu = 1$) is $\Delta \rho_{xx} \sim 0.03$ kΩ, which is considerably smaller than those in the other regions [e.g., Figs. 2(c) and 2(d)] where $\Delta \rho_{xx} \sim 0.2$ kΩ. By contrast, in the trace of Fig. 4, which shows the HFABO in the strong depletion regime, the amplitude of the h/e HFABO ($\Delta \rho_{xx} \sim 0.2$ kΩ) is comparable in magnitude with those observed in other field ranges.

In the QH plateau transition regime between $\nu = 1$ and 2, the $(N = 0, \uparrow)$ LL is bound to the antidots, while the $(N = 0, \downarrow)$ LL is either delocalized or above the Fermi level. Since the inter-LL tunneling between the extended $(N = 0, \downarrow)$ state and the bound $(N = 0, \uparrow)$ state involves spin

flip, the tunneling probability is generally low. It is rather the intra-LL tunneling between the $(N = 0, \uparrow)$ edge states of adjacent antidot that dominates the transport in this filling range. The large difference in the amplitude of HFABO between the strong and weak depletion cases (Figs. 2 and 4) is thus naturally understood in terms of the difference in the distance between the relevant edge channels belonging to the neighboring antidots, and hence in the difference in the tunneling probability.

IV. CONCLUSION

We have investigated the AB-type oscillations in antidot lattice samples in different QH regimes, using the front gate bias to control the constriction between the antidots. We have observed a few anomalous features of HFABO in the vicinity of $\nu = 2$. On the lower field side of $\nu = 2$, spin-resolved HFABO occurs with characteristic paired resistance peaks and split peak of the Fourier spectrum. Depending on the degree of constriction, the relevant process is either the inter-LL tunneling between the delocalized bulk states and the localized edge states, or the intra-LL tunneling between the bound edge states of neighboring antidots. On the higher field side of $\nu = 2$, anomalous HFABO phenomena with exotic periodicity falling between $h/2e$ and $h/3e$ are observed. Based on the comparison with the similar observations in single antidot systems, this phenomenon is interpreted basically as the $h/2e$ AB effect caused by Coulomb blockade, but modified by the fact that the relevant edge state is on the verge of delocalization. More details of the mechanism, with which charging effect affect the AB-type oscillations in the antidot array system, as contrasted to the single antidot system, are the subject of future studies.

ACKNOWLEDGMENTS

*masanori@issp.u-tokyo.ac.jp

[1] D. Weiss, M. L. Roukes, A. Menschig, P. Grambow, K. von Klitzing, and G. Weimann, Phys. Rev. Lett. **66**, 2790 (1991).

[2] K. Tsukagoshi, M. Haraguchi, S. Takaoka, and K. Murase, J. Phys. Soc. Jpn. **65**, 811 (1996).

[3] R. Schuster, G. Ernst, K. Ensslin, M. Entin, M. Holland, G. Böhm, and W. Klein, Phys. Rev. B **50**, 8090 (1994).

[4] D. Weiss, G. Lütjering, and K. Richter, Chaos, Solitons Fractals **8**, 1337 (1997).

[5] T. Ando, S. Uryu, S. Ishizaka, and T. Nakanishi, Chaos, Solitons Fractals **8**, 1057 (1997).

[6] D. Weiss, K. Richter, A. Menschig, R. Bergmann, H. Schweizer, K. von Klitzing, and G. Weimann, Phys. Rev. Lett. **70**, 4118 (1993).

[7] F. Nihey, K. Nakamura, Physica B **184**, 398 (1993).

[8] Y. Iye, M. Ueki, A. Endo, and S. Katsumoto, J. Phys. Soc. Jpn. **73**, 3370 (2004).

[9] R. Schuster, K. Ensslin, V. Dolgopolov, J. P. Kotthaus, G. Böhm, and W. Klein, Phys. Rev. B **52**, 14699 (1995).

[10] M. Kato, H. Tanaka, S. Katsumoto, and Y. Iye, Physica E (Amsterdam) **34**, 534 (2006).

[11] M. Kato, H. Tanaka, S. Katsumoto, and Y. Iye, in *Low Temperature Physics*, AIP Conf. Proc. No. 850 (AIP, Melville, NY, 2006), p. 1349.

[12] M. Kato, A. Endo, S. Katsumoto, and Y. Iye, in *Physics of Semiconductors*, AIP Conf. Proc. No. 893 (AIP, Melville, NY, 2007), p. 659.

[13] R. A. Webb, S. Washburn, C. P. Umbach, and R. B. Laibowitz, Phys. Rev. Lett. **54**, 2696 (1985).

[14] C. P. Umbach, C. van Haesendonck, R. B. Laibowitz, S. Wash-

burn, and R. A. Webb, Phys. Rev. Lett. **56**, 386 (1986).

[15] S. Ishizaka, F. Nihey, K. Nakamura, J. Sone, and T. Ando, Phys. Rev. B **51**, 9881 (1995).

[16] I. V. Zozoulenko, F. A. Maaø, and E. H. Hauge, Phys. Rev. B **53**, 7975 (1996).

[17] S. Nonoyama and A. Nakamura, Phys. Rev. B **54**, 2635 (1996).

[18] C. J. B. Ford, P. J. Simpson, I. Zailer, D. R. Mace, M. Yosefin, M. Pepper, D. A. Ritchie, J. E. F. Frost, M. P. Grimshaw, and G. A. C. Jones, Phys. Rev. B **49**, 17456 (1994).

[19] D. R. Mace, C. H. W. Barnes, G. Faini, D. Mailly, M. Y. Simmons, C. J. B. Ford, and M. Pepper, Phys. Rev. B **52**, R8672 (1995).

[20] M. Kataoka, C. J. B. Ford, G. Faini, D. Mailly, M. Y. Simmons, and D. A. Ritchie, Phys. Rev. B **62**, R4817 (2000).

[21] I. Karakurt, V. J. Goldman, J. Liu, and A. Zaslavsky, Phys. Rev. Lett. **87**, 146801 (2001).

[22] H.-S. Sim, M. Kataoka, H. Yi, N. Y. Hwang, M.-S. Choi, and S.-R. Eric Yang, Phys. Rev. Lett. **91**, 266801 (2003).